AIMS Materials Science, 5(5): 945–956.
DOI: 10.3934/matersci.2018.5.945
Received: 31 July 2018
Accepted: 14 October 2018
Published: 18 October 2018

http://www.aimspress.com/journal/Materials

Research article

Large scale production of photocatalytic TiO_2 coating for volatile organic compound (VOC) air remediation

Julien G. Mahy[1,*], Stéphanie D. Lambert[1], Jérémy Geens[1], Alain Daniel[2], David Wicky[2], Catherine Archambeau[2] and Benoît Heinrichs[1]

[1] Department of Chemical Engineering – Nanomaterials, Catalysis & Electrochemistry, University of Liège, B6a, Quartier Agora, Allée du six Août 11, 4000 Liège, Belgium
[2] AC&CS – CRM GROUP, B57, Quartier Polytech 3, Allée de l'Innovation 1, 4000 Liège, Belgium

*** Correspondence:** Email: julien.mahy@uliege.be; Tel: +3243663563.

Abstract: In this work, a pure TiO_2 colloid was produced at pilot scale of 5 L and deposited on stainless steel with a pilot roll-to-roll line to produce photocatalytic coating for VOC degradation. The pure TiO_2 colloid was synthesized with an aqueous sol–gel process, producing crystalline nanoparticles around 4–5 nm (mainly anatase phase) dispersed in water. The crystalline phases were produced at low temperature (<100 °C) without calcination step. The crystalline coating produced with roll-to-roll process was very thin, around 50 nm. The photoactivity of this coating towards VOC destruction was evaluated on the degradation of acetaldehyde; the measured activity of the coating was 35 ± 5%. With the use of mass spectrometer, it was shown that acetaldehyde was mainly converted in CO_2. The durability of the coating was assessed after 1, 2 and 3 weeks, and showed that the photoactivity stayed constant for this period.

Keywords: aqueous TiO_2; colloid; sol–gel process; pilot scale coating; photocatalysis; acetaldehyde degradation

1. Introduction

Environmental pollution has become a critical issue for our society. Atmospheric pollution, due to traffic, house heating systems or intensive industrial activities, causes public health problems, environment degradation and odor pollution [1]. Volatile organic compounds (VOCs) are an important class of air pollutants and are usually found in the atmosphere of urban and industrial areas.

Most of these compounds are known to be toxic and carcinogenic [1]. In order to eliminate these VOCs from our environment, several processes have been suggested and developed for air cleaning [2–4]. Traditional processes of purification are based on pollutant removal by simple transfer on an adsorbent phase, but the development of methods allowing the destruction *in situ* of contaminants seems to be much more efficient and advantageous for long term applications [5]. Advanced oxidation processes (AOPs) have been investigated and shown to remove pollutants from the air [2–4]. In the case of AOPs, purification techniques involve redox reactions for the degradation of organic substrates such as chemical pollutants or even micro-organisms. AOPs are not expensive, the processes are efficient at atmospheric pressure and ambient temperature, and they generally lead to a complete mineralization of the organic pollutant with a limited production of waste.

Heterogeneous semiconductor photocatalysis is an AOP which has been proven to be a promising technology for the total mineralization of most of the organic pollutants present in air or water, by using natural or artificial light [6]. It involves pollutants' adsorption on the photocatalyst surface and the oxidative degradation of these adsorbed pollutants, ideally into CO_2, H_2O and other products resulting from complete oxidation. The oxidation is performed by different active species (electrons and holes) generated in the photocatalyst under the action of an illumination [7,8]. The most frequently used photocatalyst is titanium dioxide [9], TiO_2, which is a semiconductor sensitive to UV light. The energy required for the activation of TiO_2 is high and, if natural light is used, only the most energetic fraction situated in UV wavelengths is used, which means that only 5–8% of the solar spectrum allows the activation of the catalyst [10].

Numerous studies have been undertaken and reported in the literature in the field of TiO_2 photocatalysis as immobilized catalysts in the form of thin films [11,12], the enhancement of the photocatalytic activity [13–15], the extension of the activity of the oxide toward the visible range [16,17], or the study of the mechanism and the kinetics of the photodegradation reaction of various pollutant and micro-organisms [13,18].

Due to the increasing interest of the industry in developing liquid deposition methods to replace physical vapor deposition (PVD) and plasma methods—which are known to be costly and time-consuming—the development of production and deposition processes allowing a possible up-scaling is an emerging and promising research topic.

In recent decades, the sol–gel method has proven to be an interesting approach for the synthesis of bulk TiO_2, thin films, or hybrid membrane with controlled nanostructures and surface properties [13,18–21]. Sol–gel processes are typically performed using organic solvents to prevent precipitation and complexing ligands, to lower the reactivity of the titanium alkoxide, and to facilitate the control of the evolution of the structure [12,13,22]. These reactions are followed by drying and calcination (450–600 °C) to remove the organic component and to crystallize either anatase or rutile [23].

From an industrial perspective, anhydrous organic solvent, permanent controlled atmosphere, and high temperature thermal treatments can be considered as drawbacks due to the extensive cost caused by these important requirements, making large-scale production and hence largescale application more difficult.

By using an aqueous sol–gel process, the production of undoped and doped TiO_2 does not require high temperature thermal treatments, which makes scaling-up easier [10,24,25]. Therefore,

the development of active TiO_2 photocatalytic films using an aqueous sol–gel process is a first step for large-scale industrial processing [26,27].

In this study, a large scale aqueous sol–gel synthesis of pure TiO_2 was used [26,27]. The goal was to characterize the gaseous photocatalytic activity of this material deposited with a pilot roll-to-roll line on stainless steel. The photoactivity of this material was tested in gas phase on acetaldehyde (CH_3CHO). The aim of this paper was to show the feasibility of the synthesis and deposition of sol–gel product at pre-industrial scale and the different properties that can be obtained from it, especially the gaseous photoactivity on VOCs. Indeed, the easy-to-clean nature and photocatalytic activity of this product have been shown previously on these materials [26,27]. The VOC used in this work was acetaldehyde. Acetaldehyde is a toxic, irritant and carcinogen VOC contaminant [28,29] present in indoor and outdoor environments, resulting from combustion processes [4].

2. Materials and methods

2.1. Pilot TiO_2 synthesis

The different reagents used were Titanium (IV) tetraisopropoxide (TTiP ≥ 97%, Sigma-Aldrich), nitric acid (HNO_3, 65%, Merck), isopropanol (IsoP, 99.5%, Acros) and distilled water [26,27].

Aqueous TiO_2 synthesis was scaled-up to a volume of ±5 L in a pilot glass batch reactor with a cooling system of water recirculation (jacketed reactor) [26,27]. 3.6 L of distilled water was acidified by HNO_3 to a pH equal to 1. Then, 480 g of TTiP was added to 168.8 g of IsoP, and the mixture was stirred at room temperature for 30 min. The TTiP–IsoP mixture was added to acidified water stirred by a propeller at 300 rpm. The liquid stayed under stirring for 4 h at a temperature of 80 °C, for peptization. After the reaction, a light white-blue transparent liquid sol was obtained [26,27]. The sol can be dried under ambient air flow to obtain the corresponding powder.

About 5 L of TiO_2 colloid with a concentration of 27 g/L was produced, which corresponded to about 135 g of dried pure TiO_2 powder.

2.2. Characterizations

TiO_2 nanoparticle sizes of sols were estimated by Dynamic Light Scattering (DLS) in a Viscotek 802 DLS device. This measurement gives a hydrodynamic radius of particles or the size of particle aggregates [30].

TiO_2 sol was dried under ambient flowing air to obtain powder which is used for characterizations.

The actual amount of Ti in the powder sample was evaluated by inductively coupled plasma–atomic emission spectroscopy (ICP-AES) on a VARIAN Liberty Serie II device, in order to ensure the purity and low content of organic compounds in the sample [27]. The sample underwent an alkaline fusion; the following steps were made: 0.2 g of Na-KCO_3, 2 g of Na_2O_2, and 0.2 g of sample were mixed together in a zirconium crucible [27]. Then the mixture was heated to its melting point. After cooling and solidification of the mixture, the crucible was placed in a 500 mL flask with deionized water [27]. After reaction, the crucible was removed from the flask and 6 mL of HNO_3 was added. The mixture was heated to its boiling point for 5 min, then the solution was transferred to a volumetric flask that was filled to the calibration mark with deionized water after cooling. The

solution was then analyzed using an ICP-AES device [27]. The corresponding TiO_2 powder was analyzed 3 times to ensure the reproducibility of the measurements.

The crystallographic properties of the powder were studied through the X-Ray Diffraction (XRD) patterns recorded with a Bruker D8 Twin-Twin powder diffractometer using Cu-Kα radiation. The Scherrer formula (Eq 1) was used to determine the size of the TiO_2 crystallites, d_{XRD} [31]:

$$d_{XRD} = 0.9\frac{\lambda}{(B\cos(\theta))} \quad (1)$$

where d_{XRD} is the crystallite size (nm), B the peak full-width at half maximum after correction of the instrumental broadening (rad), λ the X-ray wavelength (0.154 nm), and θ the Bragg angle (rad).

The repartition of the crystallographic phases was estimated on the powder with the Rietveld method using "Profex" software [32,33]. The amount of crystalline phase was estimated with CaF_2 internal standard (calcium fluoride, Sigma-Aldrich, anhydrous powder, 99.99% trace metal basis) also using "Profex" software [33,34].

The crystallinity has been characterized on steel substrate by grazing incidence X-Ray diffraction (GIXRD) in a Bruker D8 diffractometer using Cu radiation and operating at 40 kV and 40 mA. The incidence beam angle was 0.25 °.

The sol was deposited by roll-coating on a 316L stainless steel strip in a continuous roll-to-roll process [26]. The steel substrate was 25 cm wide, and the band length was 800 m [26], corresponding to the length of the steel coil used for the pilot test. The experiment was carried out on a pilot line equipped with an unwinder, a cleaning section, a roll-coater, an inductor for solvent evaporation, an air cooler and a rewinder (Figure 1 from [26]). The cleaning section was composed of a degreasing bath to remove dirt and an acidic bath (2 M HNO_3 solution) to increase the film adhesion by steel passivation [35]. The temperature reached by the strip in the inductor section was 100 °C [26]. The coating can be deposited at line speed ranging from 30 to 120 m·min^{-1}, allowing the amount of TiO_2 deposited to be adapted. Typically, the samples analyzed in this work were deposited at 60 m·min^{-1} [26].

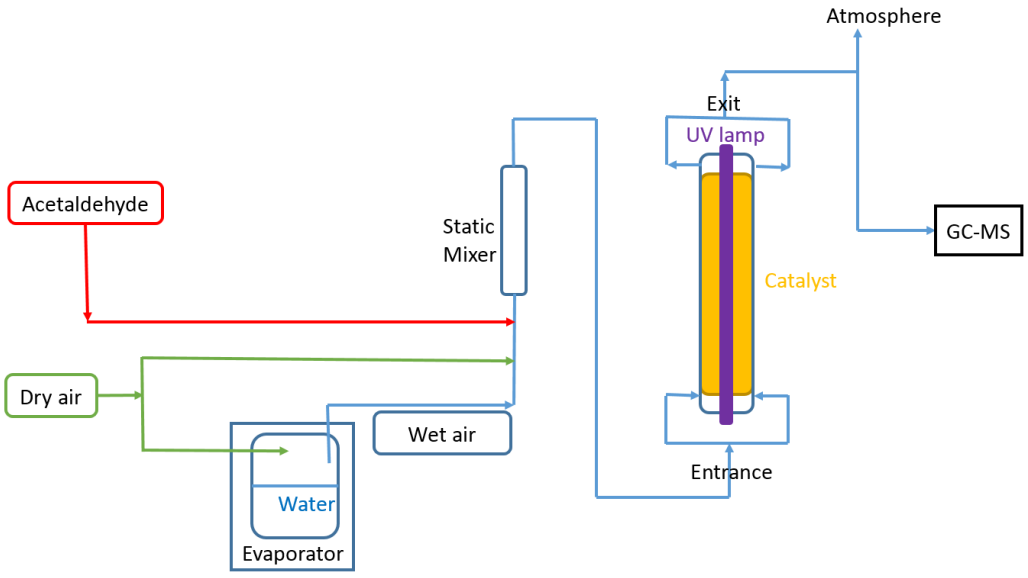

Figure 1. Gaseous photocatalytic plant.

An estimation of film thickness was done by X-ray fluorescence with an X-ray Fluorescence Spectrometer S4 PIONEER from Bruker [26]. The film adhesion was tested by rubbing the surface with a dry and a wet cloth [26].

The photocatalytic activity of TiO_2 pilot films was measured on the degradation of acetaldehyde in air [36]. The set-up was shown in Figure 1 [36]. There were three gas entrances for acetaldehyde dilute in N_2 (300 ppm), dry and wet air, one static mixer to have a homogeneous composition at the reactor entrance, the cylindrical reactor with a UV lamp inside, and a GC-MS to analyze the composition at the entrance or the exit of the reactor. The cylindrical reactor (Figure 2) was composed of three quartz tubes imbricated into each other with the UV lamp inside the small one (cylinder 1). Water circulated between cylinders 1 and 2 to keep a constant temperature through the reactor (20 °C). The polluted air flowed between the second tube and the third one, where the catalyst was also placed, defining an annular zone of reaction of 0.33 cm of a length of 30 cm [36]. The UV lamp was a UV-A light (Osram Sylvania, Blacklight-Bleu Lamp, F18W/BLB-T8), i.e., its wavelength was comprised between 315 and 400 nm. The spectrum of the lamp was measured with a photometer (mini-spectrophotometer Hamamatsu TG) and it was found that the light can be considered monochromatic with a wavelength λ = 365 nm and an intensity of 1.2 mW cm^{-2} (PMA 2100-UVA-B PMA 2107 radiometer).

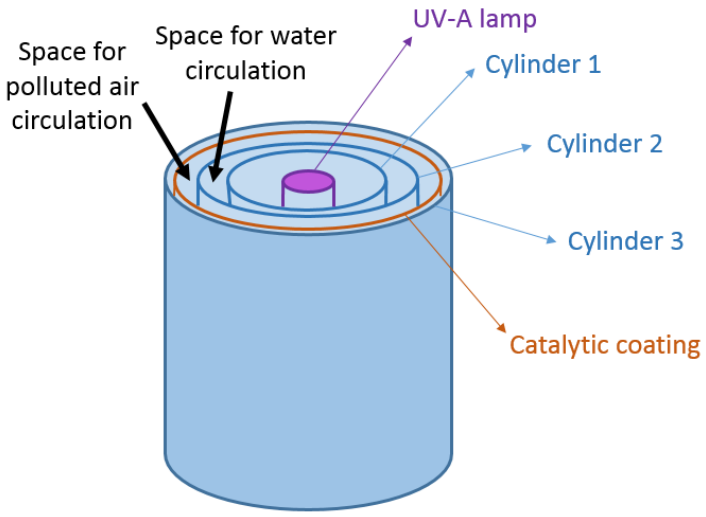

Figure 2. Cylindrical reactor.

For the photocatalytic test, the coating was in continuous contact with the polluted air, and the "in and out" concentrations of acetaldehyde were measured every 20 min during 8 h with the GC-MS by following the mass 28, 29, 30, 43, 44, 45 and 46, which corresponded to acetaldehyde and the different possible degradation compounds. The reactor needed 3 h to be stable; the measurements can be used from this time. Before catalytic tests, a calibration curve was made to ensure a linear evolution of acetaldehyde concentration for the GC-MS device between 0 and 20 ppmv. This calibration curve was obtained by changing the dilute acethadehyde gas flow (300 ppm in N_2) between 0 and 25 mL/min while keeping air flow constant to 350 mL/min.

For the catalytic test, the initial concentration of acetaldehyde was 10 ppmv, the total gas flow was 362 mL/min, only dry air was used for the tests, and the temperature was maintained at 20 °C. A

blank test without catalyst was made to show that acetaldehyde did not degrade under UV-A, and a dark test without light was made to show that no adsorption occurred during the photoactivity test. No change in the concentration was observed for the dark and blank tests. The degradation percentage was calculated by the following equation:

$$Acetaldehyde\ degradation\ (\%) = \frac{Signal_{in} - Signal_{out}}{Signal_{in}} \times 100 \quad (2)$$

where $Signal_{in}$ and $Signal_{out}$ correspond to the acetaldehyde content in the entrance and at the exit of the reactor. This equation was used when the reactor is in a stationary state.

Durability study was realized by measuring the activity of the coating on acetaldehyde degradation after 1, 2 and 3 weeks (7, 14 and 21 days) of running.

3. Results and discussion

3.1. Colloid

The produced material was a TiO_2 colloid [26,27], and the XRD pattern of the corresponding powder was represented on Figure 3. It was composed of 65% anatase, 10% brookite, and 25% amorphous fraction, calculated with CaF_2 internal calibration (Table 1) using Rietveld refinement thanks to the "Profex" software. This estimation was made only on the powder because the intensity is too weak for coating measurement.

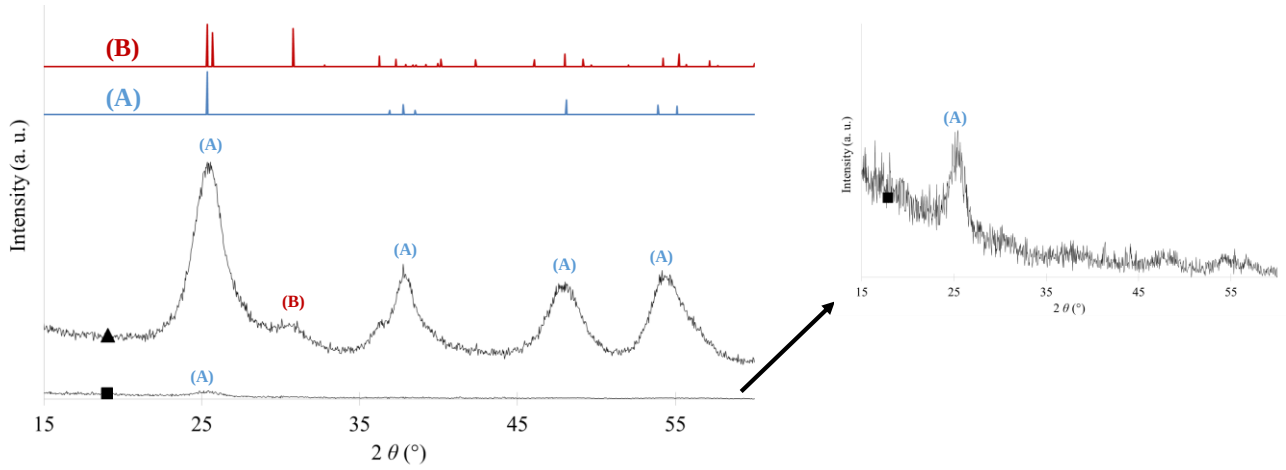

Figure 3. XRD patterns of (▲) pure TiO_2 powder and (■) pure TiO_2 coating with and without zoom, (A) reference pattern of anatase and (B) reference pattern of brookite.

The crystallite size calculated with Scherrer formula (Eq 1) was around 4 nm (Table 1).

The hydrodynamic diameter measured by DLS in the TiO_2 colloid was about 22 nm (see Table 1). The colloid was composed of nanoparticles of TiO_2 around 4–5 nm, dispersed in H_2O [26,27]. It has been shown that this material was very stable over time. Indeed, a stability study showed that the colloid kept its properties over a two-year study [37].

The purity of the sample has been assessed with ICP-AES measurements, and the Ti% were 57.9, 58.2 and 58.3 wt% respectively for the three measurements. For a pure TiO_2 material, the theoretical weight percentage of Ti was 59.9 wt%, so the sample of this work was pure and had a low content of organic compounds.

This synthesis allows for production of crystalline TiO_2 colloid without calcination step and with a very low content of organic compounds; this material is very suitable for industrial application [26,27].

Table 1. Pure TiO_2 powder, colloid and coating properties.

Sample	d_{XRD} (nm) ±1	Phase distribution (%) ±5	D_{DLS} (nm) ±5	Ep_{steel} (nm) ±5	Acetaldehyde degradation (%) ±5
Pure TiO_2	4	Am[25%] + A[65%] + B[10%]	22	50	35

d_{XRD}: mean diameter of TiO_2 crystallites measured by the Scherrer method; Am: amorphous TiO_2 phase; A: Anatase TiO_2 phase; B: Brookite TiO_2 phase; D_{DLS}: hydrodynamic diameter of TiO_2 particles aggregates measured by DLS; Ep_{steel}: TiO_2 film thickness measured with X-ray fluorescence.

3.2. Coating

The colloid was deposited on a pilot line, as described in Section 2.2. Crystalline phases of the coating were measured and depicted in Figure 3 with a zoom-in of the pattern shown on the right. The peaks of anatase were observed—as with the powder, the intensity was low because the coating is thin. The thickness (Ep_{steel}) was estimated with X-ray fluorescence which gave of 120 mg/m^2 for titanium, so the amount of TiO_2 was about 200 mg/m^2 [26]. By assuming that the coating was composed mainly of anatase phase, the density was 3.89×10^6 g/m^3 [10] and so the estimation of film thickness was about 50 nm [26] (Table 1). A nanoscale coating was well deposited with this technique. Previously, we showed that this large scale coating had easy-to-clean properties and photocatalytic activity in its liquid phase [26,27]. In this present study, we explored the photocatalytic properties in the gaseous phase.

3.3. Photocatalytic coating on gas phase

The photocatalytic activity was tested on acetaldehyde degradation (see Section 2.2), and the result of degradation was represented in Table 1 and Figure 4. The photoactivity of the scaled-up TiO_2 coating on stainless steel tested in the photocatalytic plan (Figure 1) was about 35 ± 5% of degradation of acetaldehyde (calculated with Eq 2 on Figure 4c) and stayed stable at this value when the reactor was in stationary state after about 3 h (Figure 4c). The blank and the dark tests did not show degradation or adsorption of the acetaldehyde, the decrease of the concentration was so thorough a degradation.

The mechanism of degradation of acetaldehyde can be assumed as Figure 5 [4].

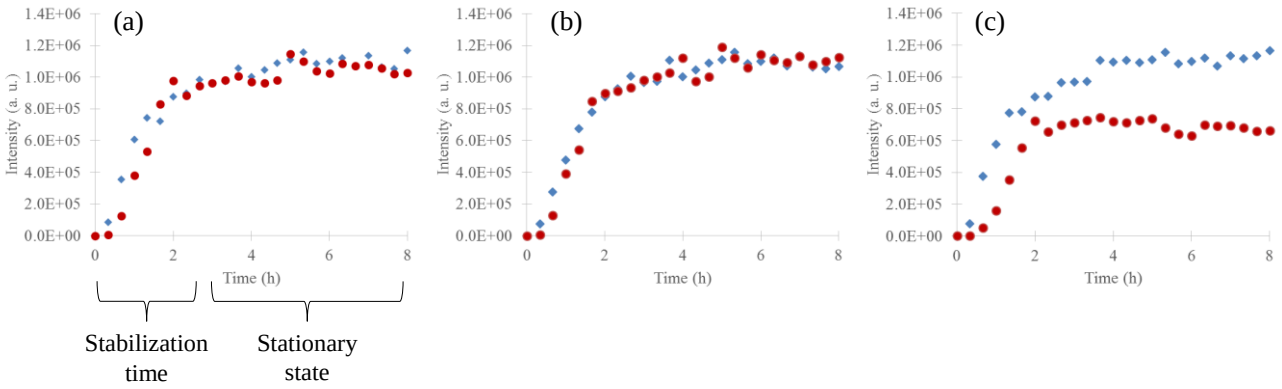

Figure 4. Evolution of the reactor (♦) entrance and (●) exit signals of acetaldehyde for (a) the blank test without catalyst, (b) the dark test without light and (c) the catalytic test with light and catalyst.

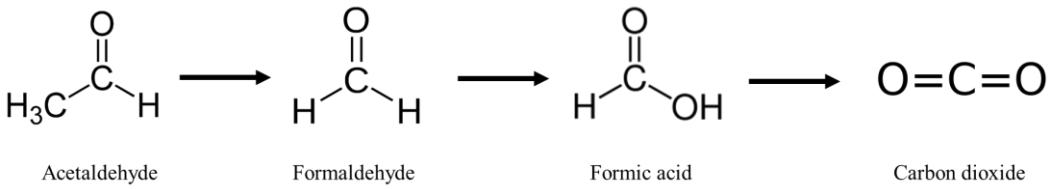

Figure 5. Degradation intermediates of acetaldehyde.

On the mass spectrometer, different masses were followed to calculate the degradation which corresponded to the different fragments of the possible molecules of the mechanism. Indeed, the masses 29, 43, 44 can correspond to the acetaldehyde [38], the masses 28, 29, 30 to formaldehyde [39], the masses 29, 44, 45, 46 to formic acid [40] and the mass 44 to CO_2 [41]. Some masses overlaid several chemical compounds, but with different conditions it was possible to calculate the different compounds during the degradation. Indeed, when we tested the device without light and catalyst, no degradation happened, all mass signals stayed constant and the signal of mass 29 was the biggest corresponding to acetaldehyde, and mass 44 was also present. When the test was made with UV light only (blank test), the concentration was not modified, and the acetaldehyde did not undergo photolysis. When the test was made with the catalyst but without light (dark test), again the signals stayed constant, and no adsorption happened. When we made the degradation test with light and catalyst, we obtained a decrease in mass 29 and an increase in mass 44; the other masses did not change very much (to <5%), so we can assume that we had a degradation of acetaldehyde mainly in CO_2 (Table 1).

The durability of the coating was assessed by measuring the degradation after 7, 14 and 21 days of running the device. The degradation after 7, 14 and 21 days was respectively 34 ± 5%, 32 ± 5% and 36 ± 5% of degradation of acetaldehyde, showing the great stability of the coating photoactivity.

With previous results on this coating [26,27], we showed that the produced coatings on stainless steel have easy-to-clean properties and photocatalytic activity in liquid and gaseous phases.

4. Conclusions

In this work, a TiO_2 colloid was produced at pilot scale of 5 L. This suspension was deposited on stainless steel with a pilot roll-to-roll line to produce photoactive coating for acetaldehyde degradation.

The pure TiO_2 colloid was composed of nanoparticles around 4–5 nm, and these nanoparticles were mainly crystalline with anatase and brookite phases. The crystalline phases were produced at low temperature (<100 ℃) without calcination step.

The coating produced with the roll-to-roll process was very thin, around 50 nm, and mainly composed of anatase TiO_2. In previous work it was shown that this material has easy-to-clean properties and a photocatalytic property in its liquid phase. In this work, the activity of the coating in its gaseous phase was explored.

The degradation of acetaldehyde measured on the coating was 35 ± 5%. With the use of mass spectrometer, it was shown that acetaldehyde was mainly converted into CO_2. The durability of the coating was assessed after 1, 2 and 3 weeks, and the photoactivity of the coating stayed constant for this period. The conditions of the test can be optimized to increase the acetaldehyde degradation.

This work was a first step for the industrialization of sol–gel product, showing that this product can be up-scaled to produce efficient coating with different properties—in this case, easy-to-clean and photocatalytic properties both in liquid and gaseous phases.

Acknowledgement

S. D. L. thanks the Belgian National Funds for Scientific Research (F.R.S.-FNRS) for her Associate Researcher position. The authors thank Isabelle Willems and Alain Germeau from Prayon S.A. for the provision of the extrapolation reactor. For their financial support, the authors are grateful to the Ministère de la Région Wallonne Direction Générale des Technologies, de la Recherche et de l'Energie (DGO6), in relation to the Plan Marshall, and with support from the Pôle MecaTech for the research project "DAO—Durable Aesthetic Outdoor Contract No. 6765".

Conflict of interest

The authors declare that they have no conflicts of interest.

References

1. Khan MA, Ghouri AM (2011) Environmental pollution: Its effects on life and its remedies. *RW-JASC* 2: 276–285.
2. Mills A, Le Hunte S (1997) An overview of semiconductor photocatalysis. *J Photoch Photobio A* 108: 1–35.
3. Paz Y (2010) Application of TiO_2 photocatalysis for air treatment : Patents' overview. *Appl Catal B-Environ* 99: 448–460.
4. Salvadores F, Minen RI, Carballada J, et al. (2016) Kinetic study of acetaldehyde degradation applying visible light photocatalysis. *Chem Eng Technol* 39: 166–174.

5. Rauf MA, Ashraf SS (2009) Fundamental principles and application of heterogeneous photocatalytic degradation of dyes in solution. *Chem Eng J* 151: 10–18.
6. Di Paola A, Garc á-L ópez E, Marc ì G, et al. (2012) A survey of photocatalytic materials for environmental remediation. *J Hazard Mater* 211–212: 3–29.
7. Bailon-Garcia E, Elmouwahidi A, Alvarez MA, et al. (2017) New carbon xerogel-TiO_2 composites with high performance as visible-light photocatalysts for dye mineralization. *Appl Catal B-Environ* 201: 29–40.
8. L éonard GLM, P àez CA, Ram írez AE, et al. (2018) Interactions between Zn^{2+} or ZnO with TiO_2 to produce an efficient photocatalytic, superhydrophilic and aesthetic glass. *J Photoch Photobio A* 350: 32–43.
9. Fujishima A, Hashimoto K, Watanabe T (1999) *TiO_2 Photocatalysis: Fundamentals and Applications*, Tokyo: KCB, Inc.
10. Malengreaux CM, Douven S, Poelman D, et al. (2014) An ambient temperature aqueous sol–gel processing of efficient nanocrystalline doped TiO_2-based photocatalysts for the degradation of organic pollutants. *J Sol-Gel Sci Techn* 71: 557–570.
11. Semlali S, Pigot T, Flahaut D, et al. (2014) Mesoporous Pt–TiO_2 thin films: Photocatalytic efficiency under UV and visible light. *Appl Catal B-Environ* 150–151: 656–662.
12. Malengreaux CM, Timmermans A, Pirard SL, et al. (2012) Optimized deposition of TiO_2 thin films produced by a non-aqueous sol–gel method and quantification of their photocatalytic activity. *Chem Eng J* 195–196: 347–358.
13. Malengreaux CM, L éonard GLM, Pirard SL, et al. (2014) How to modify the photocatalytic activity of TiO_2 thin films through their roughness by using additives. A relation between kinetics, morphology and synthesis. *Chem Eng J* 243: 537–548.
14. Di Paola A, Marc ì G, Palmisano L, et al. (2002) Preparation of polycrystalline TiO_2 photocatalysts impregnated with various transition metal ions: Characterization and photocatalytic activity for the degradation of 4-nitrophenol. *J Phys Chem B* 106: 637–645.
15. Ruggieri F, Di Camillo D, Maccarone L, et al. (2013) Electrospun Cu-, W- and Fe-doped TiO_2 nanofibres for photocatalytic degradation of rhodamine 6G. *J Nanopart Res* 15: 1982.
16. Patel N, Dashora A, Jaiswal R, et al. (2015) Experimental and theoretical investigations on the activity and stability of substitutional and interstitial boron in TiO_2 photocatalyst. *J Phys Chem C* 119: 18581–18590.
17. Di Valentin C, Pacchioni G (2013) Trends in non-metal doping of anatase TiO_2: B, C, N and F. *Catal Today* 206: 12–18.
18. Tasseroul L, Pirard SL, Lambert SD, et al. (2012) Kinetic study of p-nitrophenol photodegradation with modified TiO_2 xerogels. *Chem Eng J* 191: 441–450.
19. Carp O, Huisman CL, Reller A (2004) Photoinduced reactivity of titanium dioxide. *Prog Solid State Ch* 32: 33–177.
20. Anderson C, Bard AJ (1995) An improved photocatalyst of TiO_2/SiO_2 prepared by a sol–gel synthesis. *J Phys Chem* 99: 9882–9885.
21. Gratzel M (2001) Sol–gel processed TiO_2 films for photovoltaic applications. *J Sol-Gel Sci Techn* 22: 7–13.
22. Agartan L, Kapusuz D, Park J, et al. (2015) Effect of initial water content and calcination temperature on photocatalytic properties of TiO_2 nanopowders synthesized by the sol–gel process. *Ceram Int* 41: 12788–12797.

23. Schubert U (2005) Chemical modification of titanium alkoxides for sol–gel processing. *J Mater Chem* 15: 3701.
24. Khalil KMS, El-Khatib RM, Ali TT, et al. (2013) Titania nanoparticles by acidic peptization of xerogel formed by hydrolysis of titanium(IV) isopropoxide under atmospheric humidity conditions. *Powder Technol* 245: 156–162.
25. Mahshid S, Askari M, Ghamsari MS (2007) Synthesis of TiO_2 nanoparticles by hydrolysis and peptization of titanium isopropoxide solution. *J Mater Process Tech* 189: 296–300.
26. Mahy JG, Leonard GLM, Pirard S, et al. (2017) Aqueous sol–gel synthesis and film deposition methods for the large-scale manufacture of coated steel with self-cleaning properties. *J Sol-Gel Sci Techn* 81: 27–35.
27. Mahy JG, Lambert SD, Leonard GLM, et al. (2016) Towards a large scale aqueous sol–gel synthesis of doped TiO_2: Study of various metallic dopings for the photocatalytic degradation of p-nitrophenol. *J Photoch Photobio A* 329: 189–202.
28. Missia DA, Demetriou E, Michael N, et al. (2010) Indoor exposure from building materials : A field study. *Atmos Environ* 44: 4388–4395.
29. Zhou Y, Li C, Huijbregts MAJ, et al. (2015) Air toxics exposure and their cancer-related health impacts in the United States. *PLoS One* 10: 1–15.
30. Chu B (2008) Dynamic light scattering, In: Borsali R, Pecola R, *Soft Matter Characterization*, Berlin: Springer Netherlands, 335–372.
31. Sing KSW, Rouquerol J, Bergeret HJG, et al. (1997) Chapter 3: Characterization of Solid Catalysts: Sections 3.1.1–3.1.3, In: Ertl G, Knozinger H, Weitkamp J, *Handbook of Heterogenous Catalysis*, Wiley-VCH Verlag GmbH & Co. KGaA, 428–582.
32. Doebelin N, Kleeberg R (2015) *Profex*: A graphical user interface for the Rietveld refinement program *BGMN*. *J Appl Crystallogr* 48: 1573–1580.
33. Mahy JG, Cerfontaine V, Poelman D, et al. (2018) Highly efficient low-temperature N-doped TiO_2 catalysts for visible light photocatalytic applications. *Materials* 11: 1–20.
34. Madsen IC, Finney RJ, Flann RCA, et al. (1991) Quantitative analysis of high-alumina refractories using X-ray powder diffraction data and the Rietveld method. *J Am Ceram Soc* 74: 619–624.
35. Crookes R (2007) Le décapage et la passivation de l'acier inoxydable. Série Matériaux et application.
36. Queffeulou A, Geron L, Archambeau C, et al. (2010) Kinetic study of acetaldehyde photocatalytic oxidation with a thin film of TiO_2 coated on stainless steel and CFD modeling approach. *Ind Eng Chem Res* 49: 6890–6897.
37. Mahy JG, Deschamps F, Collard V, et al. (2018) Acid acting as redispersing agent to form stable colloids from photoactive crystalline aqueous sol–gel TiO_2 powder. *J. Sol-Gel Sci Techn* 87: 568–583.
38. Mass Spectrum of acetaldehyde, Natl. Inst. Stand. Technol. (NIST Webbook). (n.d.). Available from: https://webbook.nist.gov/cgi/cbook.cgi?ID=C75070&Mask=200#Mass-Spec (accessed July 11, 2017).
39. Mass Spectrum of formaldehyde, Natl. Inst. Stand. Technol. (NIST Webbook). (n.d.). Available from: https://webbook.nist.gov/cgi/cbook.cgi?ID=C50000&Units=SI&Mask=200#Mass-Spec (accessed July 11, 2017).

40. Mass Spectrum of formic acid, Natl. Inst. Stand. Technol. (NIST Webbook). (n.d.). Available from: https://webbook.nist.gov/cgi/cbook.cgi?ID=C64186&Units=SI&Mask=200#Mass-Spec (accessed July 11, 2017).
41. Mass Spectrum of carbon dioxide, Natl. Inst. Stand. Technol. (NIST Webbook). (n.d.). Available from: https://webbook.nist.gov/cgi/cbook.cgi?ID=C124389&Units=SI&Mask=200#Mass-Spec (accessed July 11, 2017).

AIMS Press